UCRL-16302

University of California

Ernest O. Lawrence Radiation Laboratory

THE RADIOTHERAPEUTIC POSSIBILITIES OF NEGATIVE PIONS--
PRELIMINARY PHYSICAL EXPERIMENTS

TWO-WEEK LOAN COPY

This is a Library Circulating Copy which may be borrowed for two weeks. For a personal retention copy, call Tech. Info. Division, Ext. 5545

Berkeley, California

DISCLAIMER

This document was prepared as an account of work sponsored by the United States Government. While this document is believed to contain correct information, neither the United States Government nor any agency thereof, nor the Regents of the University of California, nor any of their employees, makes any warranty, express or implied, or assumes any legal responsibility for the accuracy, completeness, or usefulness of any information, apparatus, product, or process disclosed, or represents that its use would not infringe privately owned rights. Reference herein to any specific commercial product, process, or service by its trade name, trademark, manufacturer, or otherwise, does not necessarily constitute or imply its endorsement, recommendation, or favoring by the United States Government or any agency thereof, or the Regents of the University of California. The views and opinions of authors expressed herein do not necessarily state or reflect those of the United States Government or any agency thereof or the Regents of the University of California.

The American Journal of
Roentgenology - Radium
Therapy and Nuclear Medicine

UCRL-16302

UNIVERSITY OF CALIFORNIA

Lawrence Radiation Laboratory
Berkeley, California

AEC Contract No. W-7405-eng-48

THE RADIOTHERAPEUTIC POSSIBILITIES OF NEGATIVE PIONS--PRELIMINARY PHYSICAL EXPERIMENTS

Chaim Richman, Henry Aceto, Jr., Mudundi R. Raju, and Bernard Schwartz

July 28, 1965

THE RADIOTHERAPEUTIC POSSIBILITIES OF NEGATIVE PIONS--PRELIMINARY PHYSICAL EXPERIMENTS

Chaim Richman*

and

Henry Aceto, Jr.,† Mundundi R. Raju,† and Bernard Schwartz†

July 28, 1965

Beams of roentgen rays have long been used in the treatment of cancer. Such beams were generally produced by 200- to 250-kilovolt machines. It was soon recognized, however, that roentgen rays of this energy leave much to be desired in treatment; for example, they give a high skin dose but have only limited penetrating qualities.

It was clear, therefore, that higher-energy quanta were desirable. ^{60}Co and ^{137}Cs sources and supervoltage machines have reduced the skin dose and increased the depth dose.

Cyclotrons and linear accelerators produce beams of particles with properties entirely different from those of roentgen rays and electrons, and great effort has been made to improve treatment techniques by use of these new radiations. The heavy charged particles produced by these high-energy machines--alpha particles, deuterons, and protons--undergo only small multiple-angle scattering, and can therefore be used where geometry is important. Also, such particles exhibit Bragg peaks at the ends of their ranges which can be useful in improving the ratio of dose in the tumor to dose in intervening tissue.[6,8,15] The Bragg peak is too narrow, however, to permit uniform irradiation of most tumors; furthermore, these charged particles do not have very high LET (linear energy transfer) except near the end of their travel. Variable absorbers may transform the Bragg peak into flat maxima of various lengths corresponding to the tumor dimensions, but

this distribution of particles of different energies, with its associated spread of energy over a larger volume, is achieved at the expense of the peak-to-plateau depth-dose advantage, and markedly decreases the average LET in the Bragg peak region.

When a beam of deuterons, for example, strikes a beryllium target, a useful beam of neutrons can be produced. The early work of Lawrence and co-workers suggested that neutrons, by virtue of their relatively high-LET secondary protons, produce a greater biological effect on normal and neoplastic tissue than do roentgen rays.[7]

In 1938 a beam of high-energy neutrons was first used in the treatment of advanced cancer patients,[14] but the results were not successful, owing to serious long-term damage to skin and to normal tissue, as reported by Stone.[13] More recently, Fowler et al.[4] have revived interest with a series of pretherapeutic experiments with a neutron beam, designed to elucidate the long-term injury to normal tissues reported by Stone. The recoil protons, with energies of a few MeV, give rise to ionization densities of the order of 20 keV/μ. For comparison, we note that 250-kV roentgen rays have LET's of about 3 keV/μ, and gamma rays have LET's of less than 1 keV/μ.

Pions are relatively new particles, discovered only about 15 years ago; there are positive, negative, and neutral pions. In this work we are concerned principally with negatively charged pions, or π^- mesons. The mass of the pion is between that of the electron and the proton; therefore, in passing through matter, the charged pion undergoes, in general, less Coulomb scattering than the electron and more than the proton, but in penetrating to a given range it produces less ionization per centimeter of tissue than the heavy proton. At the end of the pion range new phenomena take

place which have no counterpart with either electrons or protons. We are studying beams of pions to see if use of these unusual particles can improve on the present methods of irradiating tumors.

When negative pions come to rest in tissue, they are captured by the heavier elements--mainly carbon, oxygen, and nitrogen. This process produces an unstable nucleus, which explodes into short-range heavily ionizing fragments, resulting in an augmented Bragg curve with an enhanced peak-to-plateau ratio. The capture events can be made to take place in the tumor region by so choosing the energy of the pions that they pass through the healthy tissue and stop in the tumor. A few people, including Chaim Richman (unpublished, 1952), have appreciated this possibility. P. H. Fowler and D. H. Perkins[5] were the first to make detailed calculations of the dosage to be expected from negative pions in tumors and in the surrounding tissue. Their results show that for negative pion beams the dose delivered in the tumor should be many times that in adjoining regions. Not only is the dose at the Bragg peak greater than the skin dose, but the increased ionization at the peak, with its concomitant increase in LET, produces a greater RBE (relative biological effect) as well.

The enhanced Bragg peak has another possible advantage in radiotherapy; there is a differential between the radiosensitivity of normal tissue and of a tumor when the oxygen supply to the tumor is impaired because of poor vascularization. That is, the anoxic or hypoxic cells are not killed so readily by roentgen rays and gamma rays as are well-oxygenated healthy cells. One way of overcoming this so-called oxygen effect is to use high-LET radiation, which causes cell injury irrespective of the oxygen differential. With roentgen rays the biological effect produced is approximately three times as great under aerobic as under anaerobic conditions (i.e.,

oxygen enhancement factor ≈ 3). In contrast, this same ratio for the killing of mouse ascites tumor cells, as reported by Hornsey and Silini,[4] is 1.9 for neutrons of mean energy 6 MeV, whose average LET is approximately 20 keV/μ. The highly ionizing alpha particles, of mean energy around 6 MeV, resulting from nuclear absorption of pions in tissue nuclei should be effective in further decreasing the differential oxygen effect.

The presently available negative pion beam is low in intensity, nevertheless, some dosimetric experiments can be done quite well; with care, it may even be possible in the future to do some biological studies of the RBE and the oxygen effect for pions.

In this paper we report measurements (by ionization chambers and LiF dosimeters) of the doses from the pion beam as a function of range in a Lucite phantom. We also studied the attenuation of the beam, by counting the particles with scintillators. In addition, we measured flux-density distribution in a plane perpendicular to the beam. Of fundamental importance is the energy release in the "stars" at the end of the range; we have investigated this with silicon semiconductor detectors. Finally, we have had to take a careful look (using a time-of-flight system) at the electron background in the beam.

THE BEHAVIOR OF CHARGED PIONS IN TISSUE

Charged pions have a mass 276 times the electron mass; they weigh about 1/6 as much as protons. Unlike the electron and proton, the charged pion is unstable, and it decays in free space into a muon and a neutrino with a lifetime of $\approx 2 \times 10^{-8}$ sec. This means that for any pion beam we produce, there will be a contamination of muons.

Charged pions traverse tissue like any particle of unit electronic charge. They stop after traveling a given range that depends on energy;

e.g., a 50-MeV pion travels through about 10 cm. of tissue. In our work we usually use beams of energy around 90 MeV, which affords a good yield with a reasonable background.

To make sure that the effects we are interested in originated with the negative-pion stars, we also studied positive-pion beams of the same energy. When the positive pion comes to rest in tissue, the Coulomb repulsion between the positive charges keeps it from interacting with the nuclei. It goes through two decay processes,

$$\pi^+ \rightarrow \mu^+ + \nu,$$

followed by

$$\mu^+ \rightarrow e^+ + \nu + \bar{\nu}.$$

The ν and $\bar{\nu}$ are neutrinos and do not contribute to dosage. The μ^+ is a short-range 4-MeV muon, which contributes a small dose. The positron in the second equation has a beta-spectrum energy distribution with a peak around 30 MeV, and a maximum of around 54 MeV.

The negative pion behaves differently from the positive pion: when a negative pion comes to rest, it is captured (because of its negative charge) by an atom in the tissue, and it cascades down the atomic levels of the atom in a time short compared with its lifetime. From the lowest atomic level it is captured by the nucleus, and the nucleus then explodes.

The type of breakup that one gets with the light nuclei has been studied by Ammiraju and Lederman,[1] using a diffusion cloud chamber. They find that the release of energy in the ionizing fragments is particularly favorable in the light elements. For carbon the dominant reaction (39% of the captures) turns out to be

$$\pi^- + {}^{12}C \rightarrow 2\,\alpha + 1\,p + 3\,n,$$

where α represents an alpha particle, p is a proton, and n a neutron. In nitrogen, the dominant reaction (34% of the captures) is

$$\pi^- + {}^{14}N \rightarrow 3\alpha + 2n.$$

The other reactions yield from 0 up to 5 charged particles, at times including a heavy ion. A few examples of this capture and resulting explosion as observed in nuclear emulsion[10] are shown in Fig. 1. The alpha particles and protons have ranges of only a few mm. in tissue, and the neutrons produced here can be expected to contribute only a small dose to the tissue.

We see from these considerations that negative pions should have many advantages over roentgen rays, protons, or neutrons. They have an excellent ratio of depth dose to skin dose. They traverse the healthy tissue with a low LET, and only in the tumor region does the LET become high. Here low-energy alpha particles and protons are formed, and the average LET is about 50 keV/μ. From experiments with other radiations we know that the RBE increases with LET in this region, and that the absence of oxygen in a tumor has a smaller effect on the radiosensitivity of the tumor.

THE PRODUCTION OF BEAMS OF NEGATIVE AND POSITIVE PIONS

Pions are secondary particles, and in our experiments they were produced by the Berkeley 184-inch synchrocyclotron. This machine provides an intense beam of 732-MeV protons that in their outer orbit strike a 2-inch beryllium target and produce neutral, positive, and negative pions. The experimental arrangement is shown in Fig. 2. The negative pions are deflected out of the cyclotron by the cyclotron fringe field itself, and after leaving the cyclotron tank through a window, go through a small quadrupole focusing magnet, then along a channel through the main cyclotron shielding. Thereafter the pions enter a large shielded room called the meson cave, where various arrangements of magnets are used to bend and focus the pion beam.

It is common to use a bending magnet followed by a quadrupole focusing magnet; frequently, however, we have used the bending magnet alone, which removes particles of different $H\rho$ from the pions that are being used. The cyclotron produces pions in a range of energies from 0 up to about 450 MeV; in our experiments, we used pions of 90 MeV, which have a range of 24 cm. of tissue.

The negative pions that come off in the direction of the proton beam are bent oppositely to the protons and out of the cyclotron. The positive pion beam consists of pions that come off backward to the proton beam. In general, their intensity is lower. In the change from a negative to a positive pion beam, all the magnetic fields are reversed, including that of the cyclotron. The magnetic lens system remains unchanged for pions of the same energy. The target settings were taken from the report of Astbury et al.,[2] the radius and azimuth of the target were adjusted slightly from these values to maximize the beam intensity.

The negative pions are produced in the reaction of the beam with the neutrons in the beryllium nucleus:

$$p + n \rightarrow p + p + \pi^-.$$

The positive pions are produced in two ways:

$$p + n \rightarrow n + n + \pi^+,$$

$$p + p \rightarrow p + n + \pi^+.$$

The charged pions all have the same lifetime. The neutral pions have a very short lifetime, $\approx 10^{-16}$ sec., and decay into two 70-MeV gamma rays in the target, where they convert and give rise to electron-positron pairs that are mainly in the forward direction. The electrons from this conversion constitute the principal background in the negative-pion beams.

BEAM PROFILES

An important parameter for a pion beam is the flux-density distribution in a plane perpendicular to the beam. An appraisal of this was made from horizontal and vertical profiles of the pion beam obtained by the beam-profile counter of Solomon and Andreae.[12]

Two thin 2-inch-diameter plastic scintillation monitor counters, in double coincidence, are mounted one behind the other and aligned with the central axis of the beam. They give a counting rate proportional to the incident flux. A pair of "beam finder" scintillation counters 3/8 inch thick and 1.5 inches in diameter served to provide a double-coincidence measurement of the intensity at points at various distances from the central axis, at right angles to the beam. The "beam finder" counters move over a 7-inch linear path normal to the beam axis, taking a measurement every 0.1 inch. The number of beam-finder counts per unit incident flux at every 0.1 inch is consecutively stored in 70 channels of the TMC 400-channel pulse-height analyzer (PHA), and subsequently recorded on the associated printout mechanism.

Figure 3 shows the results of a study of the horizontal beam profile of one of our beams without absorbers and with 4 and 7.5 inches of Lucite absorbers in the beam. It is clear that the absorbers produce a large lateral spreading of the beam, with a corresponding reduction in the peak intensity.

INTEGRAL RANGE CURVE

As the pion beam passes through matter it is attenuated by virtue of the elastic and the inelastic processes with the nuclei of the medium. The beam also undergoes multiple Coulomb scattering. Consequently the number of particles decreases as the thickness of absorber increases. This particle loss is extremely important, since the dose available at the Bragg peak

depends on the intensity. In order to evaluate these losses in the beam for negative pions it is common to study the integral range curve.

The apparatus consists of three 4×4×1/8-inch plastic scintillators operating as particle counters, and associated electronics (see Fig. 4). The front two monitor counters, operated in double coincidence, define the beam intensity, including the contaminants. A variable absorber is then placed between the first two counters and the third counter, and a transmission-type measurement is made of the beam intensity as a function of the absorber thickness, which is expressed in the triple coincidences between all three counters. The integral range curve is the plot of the number of triple coincidences divided by the double coincidences (the incoming beam intensity) as a function of the absorber thickness. This is shown in Fig. 5.

Between zero absorber thickness and point A on the curve we see the attenuation of the beam before the pions stop, which for this beam was 40% of the original particles. From point A to point B, there is a sharp drop-off in intensity, because the pions stop in this region; the dose is a maximum in this region. From point B on, we see the muon and electron contaminations.

The average energy, energy spread, and degree of muon and electron contamination were also determined by this integral range method. An average pion energy of 101 MeV (196 MeV/c) was found for this beam setup by taking the average of the energies corresponding to the pion ranges at points A and B (94.5 and 108 MeV, respectively) of Fig. 5. The spread in the pion energy is ±6.75 MeV, which corresponds to a spread in momentum of ±8.4 MeV/c. The muons in the final beam, resulting from the decay of pions before the beam reaches the analyzing magnet, have the same range of momentum as the pions. Because of their mass difference, pions and muons

of the same momenta have different energies. In this case, the momenta correspond to a range of muon energies (point B to point C) which extends from 100 to 123 MeV, with an average energy of 116 MeV. These muons have a range about 30% greater than the pions. If the muon contamination represents a sizable fraction of the total beam, it may seriously affect the localization of energy. For this pion beam this contamination is approximately 10%. The electron contamination can be estimated from the curve as 25% of the beam. According to the integral-range data, the maximum intensity for this particular beam, after correction for the muon and electron contamination, is 2×10^4 negative pions per cm^2 per sec.

The time-of-flight experiment throws further light on these contaminations in the beam.

MEASUREMENTS WITH IONIZATION CHAMBERS‡

The first dosimetric exposures to the beam were made with a Lucite phantom with sheets of roentgen-ray film placed between the slabs that made up the phantom. The film shows that the pion beam travels about 8 inches in Lucite, as expected. Beyond the range of the pions there is a background of radiation visible on the film.

An ionization chamber 7 inches in diameter was used to maximize and monitor the beam; it was filled with a mixture of 96% argon and 4% carbon dioxide, at a pressure of 2 psi over atmospheric pressure. The saturation voltage was 1000 volts.

We studied the pion beams by using one chamber as a monitor followed by different thicknesses of Lucite absorber and the second chamber as a detector. These first chambers were 2 inches deep in the beam direction, and used copper windows 5 mils thick.

Measurements were made for beams of both negative and positive pions. The Bragg peak for negative pions should be greater than and of somewhat different shape from that for positive pions. The difference between the two peaks is essentially although not strictly a measure of the energy deposited in the chamber from capture events in the negative pion beam.

Figures 6 and 7 show the results of these experiments, where the measurements of the pion beam in the detector chamber (I) have both been normalized to the monitor chamber (I_0). We note that with the positive pions there is very little background, but with the negative pions there is an appreciable background. This is understandable, since the positive pions are taken off backward from the proton beam to get them out of the cyclotron, while negative pions are taken off in the direction of the proton beam. The electrons and positrons are mainly forward.

To compare the two curves, we must subtract the backgrounds. The electrons undergo a great deal of multiple Coulomb scattering, and their contribution can vary at different thicknesses of absorber. As a first-order approximation we have taken the broad muon and electron plateau regions of the curve persisting beyond the Bragg peak to be the background at all points in the absorber. This gives a 40% background to be subtracted for the negative pion beam. The resulting curves, normalized to unity for zero absorber thickness, are shown in Fig. 8.

There is a difference in both shape and height of the two curves; the Bragg peak intensity for negative pions is 20% above that for positive pions. Furthermore, the negative pion peak has been shifted to the right of the typical Bragg peak, as represented by positive pions. The new position of the peak corresponds roughly to the range of 90-MeV pions.[11] This region

also represents the place where most of the pions are stopping, and should show the contribution from the pion capture.

The interpretation of these curves is not as simple as one would like: first of all there is the uncertainty introduced by the background; then there is the fact that the nuclear fragments that are produced have ranges in our chamber which are much larger than the size of the chamber. This means that wall effects can be important. To study these effects we built a 15-atmosphere chamber and filled it with nitrogen to simulate more closely the light nuclei in tissue. Within the accuracy of our experiments we found no difference between the results with this chamber and the first chambers.

The peak dose is not so much larger than the entrance dose for negative pions as one might expect; however, more work needs to be done with improved beams.

The average dose found in one of our beams was about 8 rad/hour, including the contaminations. This dose was also measured with LiF dosimeters and found to be about 8 rad/hour, with a peak-to-plateau ratio, again, of around 3:1. The dose distribution observed with these dosimeters confirms in a rough way the shape of the peak as observed with the ionization chambers; it must be added, however, that the LiF dosimeters have a basic limitation in the Bragg region, for they show a reduction in sensitivity of as much as 40% for high-LET radiations, so that the peak-to-plateau dose is probably higher than is indicated by these dosimeters.

SEMICONDUCTOR DETECTORS

Semiconductor detectors are widely used because of their many advantageous properties. One of the most attractive features of these detectors is that the output is linearly proportional to the energy deposited.[13]

It is very important to know the energy distribution of the pion stars and to have a better measurement of the ratio of dose delivered at the end of the range to that at the entrance. Some measurements of the energy of the star fragments have been made with the diffusion cloud chamber[1] and emulsions.[9] In this study we have extended these measurements to include two different types of semiconductor detectors—a silicon surface-barrier-type detector and a lithium-drifted detector.

The experimental setup for both semiconductor detectors is shown in Fig. 9. The test pulse generator used in the system was calibrated by using an ^{241}Am source, a ^{207}Bi internal conversion electron source, and particles from the heavy-ion accelerator. The surface-barrier detector was calibrated by using the ^{241}Am source only, while the lithium-drifted detector calibration involved both sources. Lithium-drifted detector experiments with alpha particles from the 184-inch cyclotron confirm the linearity of the system up to 85 MeV. The depletion layer of the surface-barrier detector was chosen to correspond to the range of the nuclear fragment of greatest importance to us---the alpha particle. The depletion layer thickness was 4.54×10^{-2} gm./cm.^{2}, sufficient to absorb most of the alpha particle fragments. This thickness of silicon corresponds roughly to the ranges of a 20-MeV alpha particle, a 5-MeV proton, and a 0.22-MeV electron. Hence, a sizable portion of the nuclear energy released via protons escapes from the detector. Likewise, the contribution to the detector response by the incident pions, muons, and electrons is small. For any thickness of Lucite absorber, the total energy deposited in the depletion layer of the detector is given by the integral over all the channels of the product of energy per channel and the total counts in that channel.

The relative value of the energy absorption at the peak compared with that at the entrance (i.e., tumor-skin ratio) is approximately 17:1, nearly

six times the tumor-skin ratio measured with the ion chamber. Since the detector response has been maximized for response to the alpha fragments, this sizeable increase in energy deposition is due mainly to the alpha particles from the star events. In the light of the detector limitations, this ratio has little value as an absolute number; it sets an upper limit to the tumor-skin ratio.

The depletion region can be increased considerably by using a lithium-drifted silicon detector. Figure 10 shows the response of the unattenuated 180-MeV/c negative pion beam with its muon and electron contaminations of the same momenta. Two peaks, one at 0.87 MeV and the other at 1.05 MeV, are clearly visible. They are due to electrons and pions, respectively. The muon contamination, being small, is perhaps hidden in the distribution of the electrons and pions.

The width of the Bragg peak at the 50% level as determined by the ionization chambers is approximately 1.8 gm./cm.^{2} of Lucite. The thickness of the semiconductor is 0.61 gm./cm.^{2}. Hence, if the detector is sitting at the Bragg peak position, a good portion of the pions is stopped in the detector and creates stars in silicon. In order to see the energy distribution of the pion stars alone, the energy deposited by the pions, muons, and electrons through the detector has to be eliminated. When we add another semiconductor detector in anticoincidence with the analyzing detector, we observe only the pions that stop in the analyzing detector (i.e., pion stars), and the rest of the events can be eliminated. However, sometimes, one of the prongs of the stars in the first detector can pass through the second detector and cause an anticoincidence, thereby losing some stars. This does not affect the energy distribution of the pion stars appreciably. Figure 11 shows the energy distribution of the pion stars. The upper curve is the

distribution obtained without using the second detector in anticoincidence. The bottom curve is obtained by using the anticoincidence detector, thereby giving the energy distribution of pion stars in silicon. Since the thickness of the detector corresponds to the range of approximately 84-MeV alpha-particles and 20-MeV protons, this energy distribution of pion stars is not the total energy of the star but only that fraction of the energy of the star fragments deposited in the detector. Most of the alpha particles are stopped in the detector. Indeed, this is also true for the protons, except that some of the higher-energy protons may deposit only a small amount of their energy. On the other hand, neutrons escape the detector most of the time. It can be seen from the figure that the number of stars is a constantly decreasing function with energy, and that this star energy extends beyond 60 MeV. Since both curves are taken for the same amount of charge collected in the monitor, strictly speaking they should coincide down to low energies. However, the lower curve (for anticoincidence detection) is less than the upper curve (for single detector), thereby indicating that some of the star events are lost when the anticoincidence detector is used, because some of the fragments pass through the analyzing detector and reach the anticoincidence detector.

A calculation similar to that for the surface-barrier detector gives the energy deposited in the detector.

This method applied to the curves of Figs. 10 and 11 gives the energy deposited in the detector on the plateau and in the Bragg peak region; the ratio of the two, for the same total flux of incident particles, is the tumor-skin ratio. The energy deposited in the silicon detector at the Bragg peak position, by this method, is about 12 times that at the entrance (i.e., tumor-skin dose ratio equals 12). It should be mentioned that this ratio was obtained by collimating the pion beam with a 2-in.^{2} lead collimator upstream from the steering magnet.

Later measurements with an uncollimated pion beam revealed a tumor-skin ratio of about 3:1, and even less. The amount of collimation used upstream from the steering magnet is important, since for equal settings of the steering magnet, this collimation determines the momentum spread of the beam. It can be seen that the tumor-skin dose ratio is a very sensitive inverse function of the momentum spread.

TIME OF FLIGHT

Our concern with the background radiation in the pion beam led us to a different approach. This method measures the time taken by each particle in the beam to traverse an extended path (which, in the setup in the pion cave, was approximately 23 feet). This system, developed by Nunamaker and co-workers, uses a 4×4×1-inch plastic scintillator at each end of the flight path. The geometry of this experiment is therefore different from the other experiments. The velocity spectrum of the particles, as expressed by the time delay between the two detector responses, is fed to a time-to-pulse-height converter and then to a PHA. The results were photographed on the cathode-ray tube.

Figure 12 shows four Polaroid pictures of the PHA display for a negative pion beam after passing through 2-1/8, 6-1/8, 8-5/8, and 13-1/8-inches of Lucite absorber. For 2-1/8 and 6-1/8 inches of absorber, the beam is clearly differentiated into three distinct peaks representing the pions, muons, and electrons. Summation of a single peak gives the total number of particles represented by that peak. This procedure was repeated at several different depths in Lucite. One finds that the variation of the electron component with distance is similar to the exponential function obtained by using the integral range method. That is, both systems reveal a loss of about 25% of the electrons in traversing a distance equal to the range of the pions in Lucite. This is shown in Fig. 13. The percentage of electrons in the total beam of momentum 180 MeV/c increases

linearly from 23% at the surface to 40% at the Bragg peak position in Lucite. These results agree well with the integral range data.

CONCLUSIONS

This study of the physical properties of a negative pion beam shows that we can learn a great deal about these beams with the presently available intensities.

The different detection techniques and the different experiments have thrown light on the properties of such a beam. We have seen that the Bragg peak for a negative pion beam, as measured with a 1-atmosphere argon-carbon dioxide chamber, gives a peak-to-plateau ratio of around 3:1. This ratio is not so high as we expected; however, the ionization chamber is not the appropriate detector for the stars, because the ranges of the nuclear fragments are frequently longer than the depth of the chamber. The semiconductor detectors are more appropriate for these phenomena; they give, in general, higher peak-to-plateau ratios.

The energy distribution of the stars has been determined very clearly for silicon.

We have utilized 90- to 100-MeV beams; a better beam for our work would be a 50-MeV beam, having a range of 10 cm. of tissue; this would obviate the large amount of slowing down of the particles with concomitant attenuation and scattering.

The large background of electrons and smaller background of muons obscure the nature of a beam. We hope to add an electrostatic separator in our experimental setup to remove these radiations.

Taken all together, a lower-energy pion beam free of contaminations would make it possible, with the techniques that we have used to look more carefully at the characteristics of negative pion beams.

Finally we hope in the future to study the biological effects of pions, especially to the response of oxygenated and anoxic cells to the pion stars.

ACKNOWLEDGMENTS

It is a pleasure to thank many people who have made it possible for us to do this work. First and foremost we are indebted to Dr. J. H. Lawrence and Dr. C. A. Tobias, who invited us to work in Berkeley on the 184-inch synchrocyclotron and have helped us in many ways. We are also grateful to many members of Donner Laboratory for their continuous help, especially Messrs. Nick Yanni and Howard Maccabee.

The effectiveness and help of the cyclotron crew under the direction of Mr. James Vale has made our work much easier. We also want to thank Steve Richman for his help with the experimental work.

Dr. F. J. Bonte of Southwestern Medical School has been generous with advice and encouragement. In addition, a number of people in Dallas have been most helpful, especially Mr. J. S. Robottom, Dr. Robert Sippel, Dr. Bill Burke, Dr. Henry Lanz, and Dr. William Zebrun.

One of us (H. A.) is indebted to the Gilbert X-Ray Co. for a Gilbert X-Ray Co. Predoctoral Fellowship in Radiation Physics and Radiation Biology.

We are indebted to Dr. C. F. Powell, Dr. P. H. Fowler, and Dr. D. H. Perkins for the use of the excellent photograph from their book (see reference 10).

Our sincere thanks go to the American Cancer Society, and the U. S. Atomic Energy Commission, whose confidence and support have made it possible to initiate and continue this work.

FOOTNOTES

*Graduate Research Center, P. O. Box 30365, Dallas, Texas.

†Donner Laboratory and Donner Pavilion, University of California, Berkeley, California.

‡An account of these results appeared in the "Semiannual Report, Biology and Medicine, Donner Laboratory and Donner Pavilion," Lawrence Radiation Laboratory Report UCRL-11387, Spring 1964.

1. Ammiraju, P., and Lederman, L. M. A Diffusion Chamber Study of Very Slow Mesons. IV. Absorption of Pions in Light Nuclei. Nuovo Cimento, 1956, 4, 283-306.

2. Astbury, A., Crowe, K. M., Deutsch, J. G., Maung, T., and Taylor, R. E. Study of the Optimum Target Position for the Secondary Meson Beams from the 184-inch Cyclotron. UCRL-10120 (Internal distribution), 1962, March 14.

3. Bromley, D. A. Semiconductor Detectors in Nuclear Physics, Nuclear Science Series Report No. 32, Semiconductor Nuclear Particle Detector, 1960, 61-73.

4. Fowler, J. F., Morgan, R. L., and Wood, C. A. Pre-therapeutic Experiments with the fast Neutron Beam from the Medical Research Council Cyclotron, A Symposium given at the Annual Congress of the British Institute of Radiology 1962, April 27. Brit. J. Radiol. 1963, 36, 77-80.

5. Fowler, P. H., and Perkins, D. H. The Possibility of Therapeutic Applications of Beams of Negative π-Mesons. Nature 1961, 189, 524-528.

6. Larsson, B. Pre-therapeutic Physical Experiments with High Energy Protons. Brit. J. Radiol. 1961, 34, 143-51.

7. Lawrence, J. H., Aebersold, P. C., and Lawrence, E. O. The Comparative Effects of Neutrons and X-Rays on Normal Neoplastic Tissue, in "Some Fundamental Aspects of the Cancer Problem" Symposium. Am. Assoc. Adv. Sci., Occasional Pub. No. 4 1937, 215-219.

8. Lawrence, J. H., Tobias, C. A., Born, J. L., Gottschalk, A., Linfoot, J. A., and Kling, R. P. Alpha Particle and Proton Beams in Therapy. J. Am. Med. Assoc. 1963, 186, 236-45.

9. Menon, M. G. K., Muirhead, H., and Rochat, O. Nuclear Reactions Produced by Slow Negative Pi-Mesons. Phil. Mag. 1950, 41, 583-618.

10. Powell, C. F., Fowler, P. H., and Perkins, D. H. The Study of Elementary Particles by the Photographic Method (New York, Pergamon Press, 1959), 669 p.

11. Rich, M., and Madey, R. Range-Energy Tables, University of California Radiation Laboratory Report UCRL-2301, 1954 March (unpublished).

12. Solomon, J., and Andreae, S. W. Beam-Profile Detector. Rev. Sci. Instr. 1963, 34, 1126-1129.

13. Stone, R. S. Neutron Therapy and Specific Ionization. Amer. J. Roentgenol. 1948, 59, 771-785.

14. Stone, R. S., Lawrence, J. H., and Aebersold, P. C. Use of Fast Neutrons in the Treatment of Disease. Radiology 1940, 34, 322-327.

15. Tobias, C. A., Anger, H. O., and Lawrence, J. H. Radiological Use of High Energy Deuterons and Alpha Particles. Amer. J. Roentgenol. 1952, 67, 1-27.

LEGENDS FOR ILLUSTRATIONS

Fig. 1. Examples of the capture of negative pions and the resulting nuclear disintegrations in the light elements carbon, nitrogen, or oxygen as observed in nuclear emulsions. The pion tracks are labeled π^-; the stars produced following their capture have various numbers of prongs.

Fig. 2. The production of a negative pion beam. For the production of a positive pion beam all the magnetic fields are reversed and the direction of the proton beam is reversed.

Fig. 3. Horizontal profiles of one of the negative pion beams after 0, 4, and 7.5 inches of Lucite, as measured with particle counters.

Fig. 4. Block diagram for the integral range experiment.

Fig. 5. The integral range curve for a negative pion beam of about 100 MeV.

Fig. 6. The Bragg-type curve for a negative pion beam. The contaminations can be seen in the ionization beyond the main peak.

Fig. 7. The Bragg-type curve for a positive pion beam. In this beam the contaminations are quite low, as can be seen by the low ionization beyond the main peak.

Fig. 8. A comparison of the Bragg-type curves for negative and positive pions, with the contaminations subtracted to a first approximation.

Fig. 9. Block diagram of electronics for the pulse-height analysis of a pion beam with semiconductor detectors.

Fig. 10. The unattenuated negative pion beam as seen by lithium-drifted silicon detectors. The electron peak is at 0.87 MeV and the pion peak is at 1.05 MeV.

Fig. 11. The energy distribution of the negative pion endings in silicon, which is very nearly the energy distribution of the pion stars. The curve without the anticoincidence detector includes the pulses of particles passing through but not stopping in the analyzing detector.

Fig. 12. The time of flight of the different particles in the negative pion beam after different thicknesses of Lucite absorber: 2-1/8, 6-1/8, 8-5/8, and 13-1/8 inches. The scale setting on the PHA was 10^4 counts full scale for the run with 2-1/8 inches of Lucite, but 3×10^3 counts full scale for the others.

Fig. 13. The number of electrons as a function of distance in the absorber, calculated from the time-of-flight data.

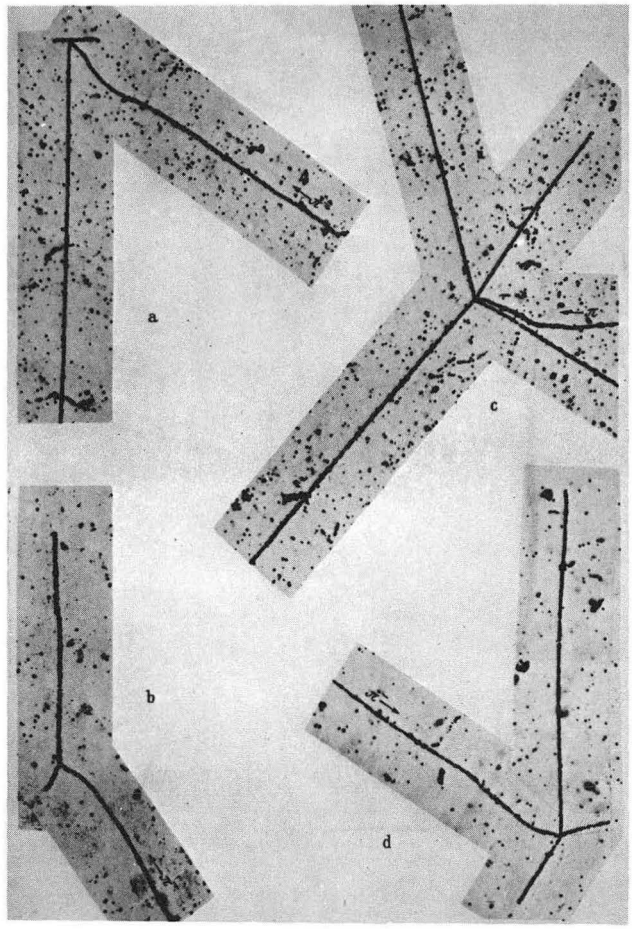

ZN-5089

Fig. 1

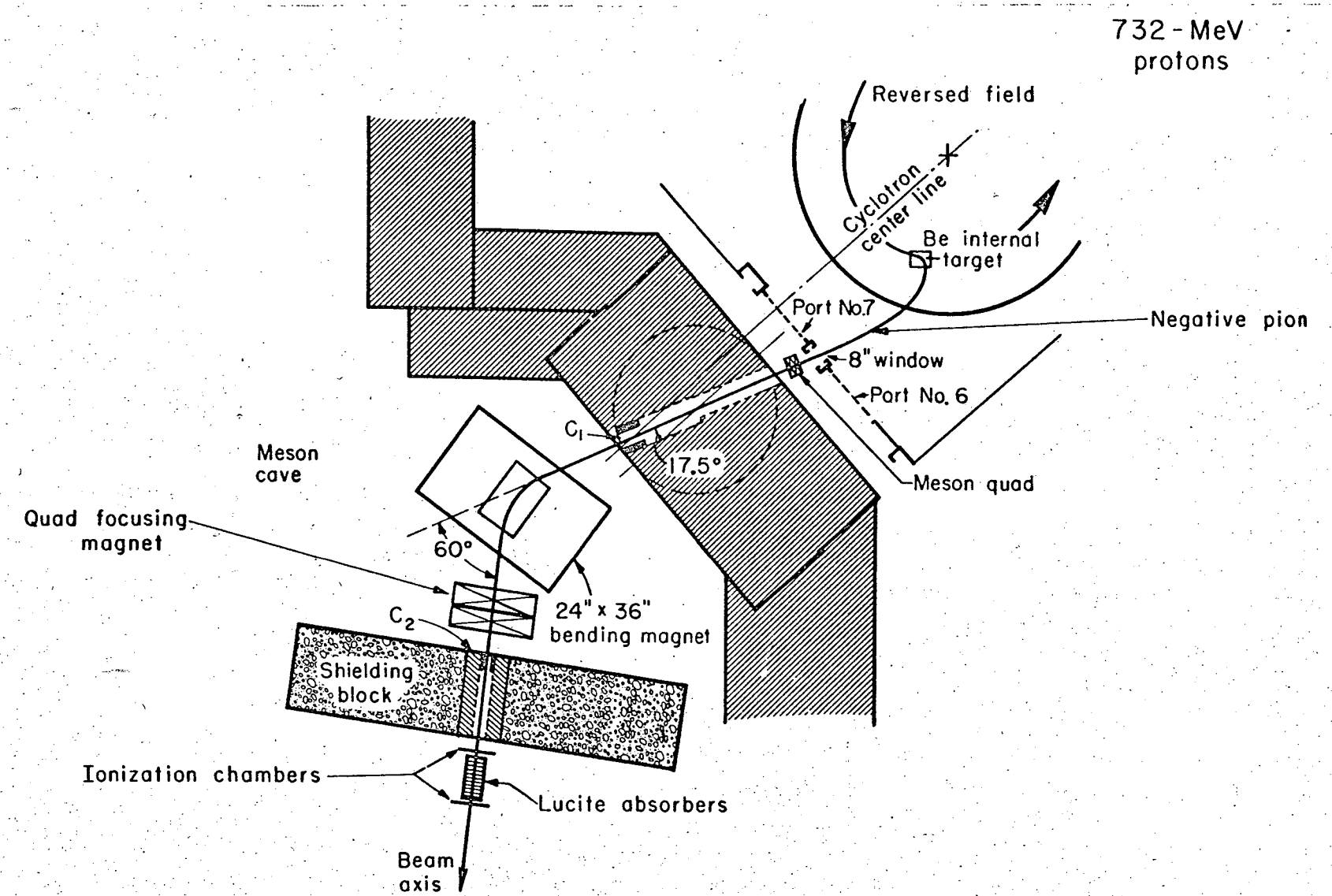
732 - MeV
protons
Reversed field
Cyclotron
center line
Be internal
target
Port No.7
Negative pion
8" window
Port No. 6
Meson quad
C_1
17.5°
Meson
cave
Quad focusing
magnet
60°
24" x 36"
bending magnet
C_2
Shielding
block
Ionization chambers
Lucite absorbers
Beam
axis

Fig. 2

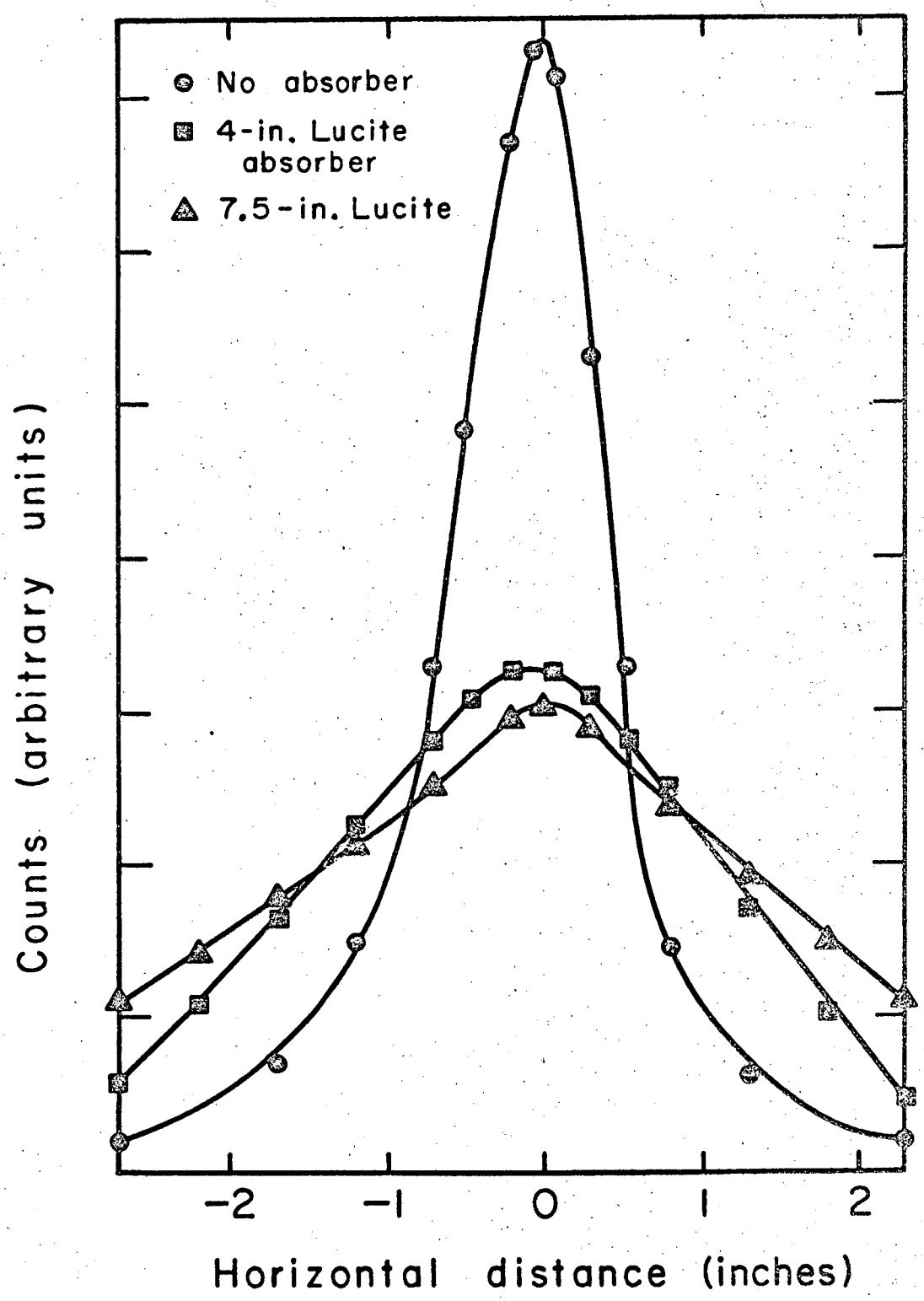
No absorber
4-in. Lucite absorber
7.5-in. Lucite
Counts (arbitrary units)
-2
-1
0
1
2
Horizontal distance (inches)

Fig. 3

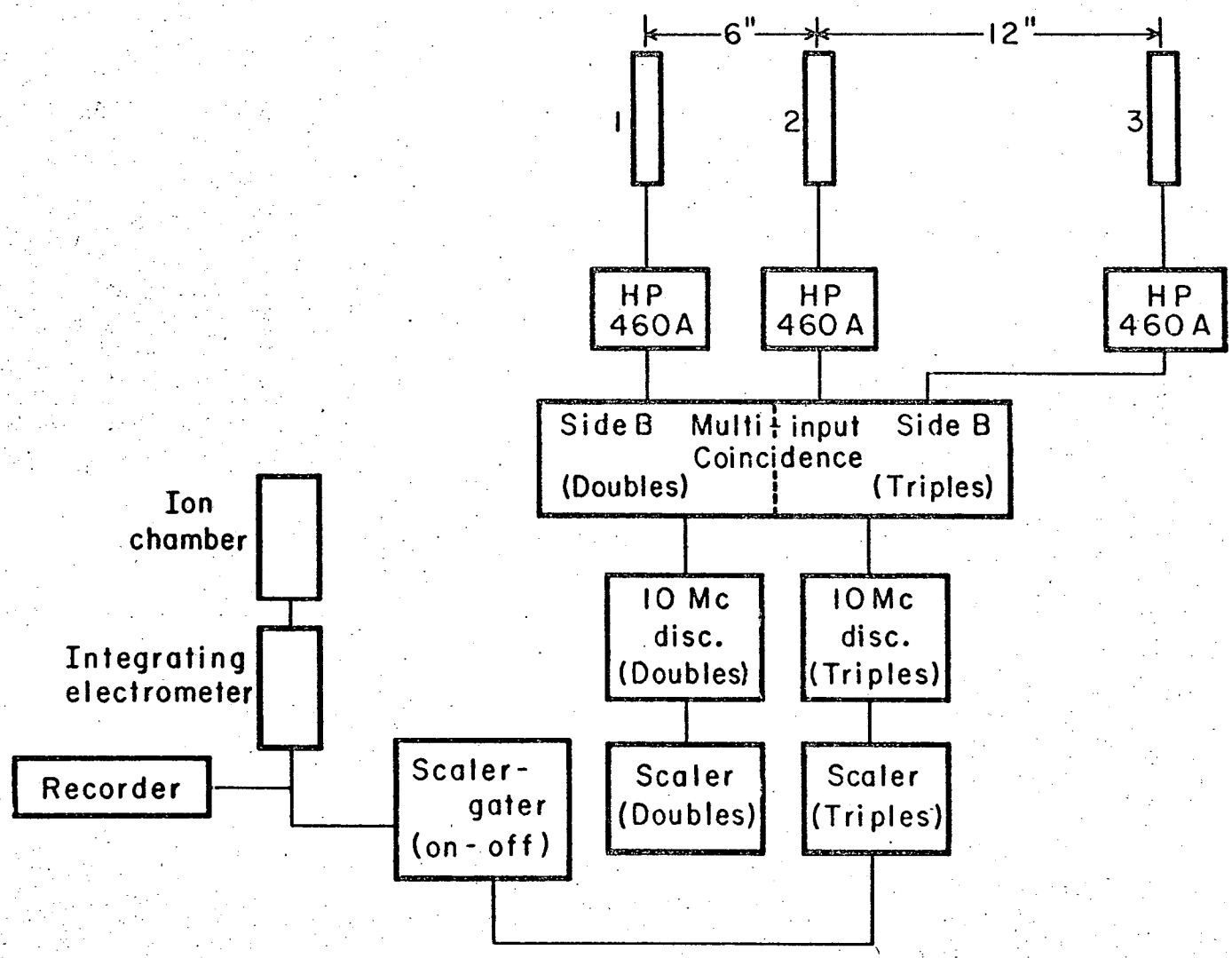
6"
12"
1
2
3
HP 460A
HP 460A
HP 460A
Side B (Doubles)
Multi-input Coincidence
Side B (Triples)
Ion chamber
Integrating electrometer
Recorder
Scaler-gater (on-off)
10 Mc disc. (Doubles)
10 Mc disc. (Triples)
Scaler (Doubles)
Scaler (Triples)

Fig. 4

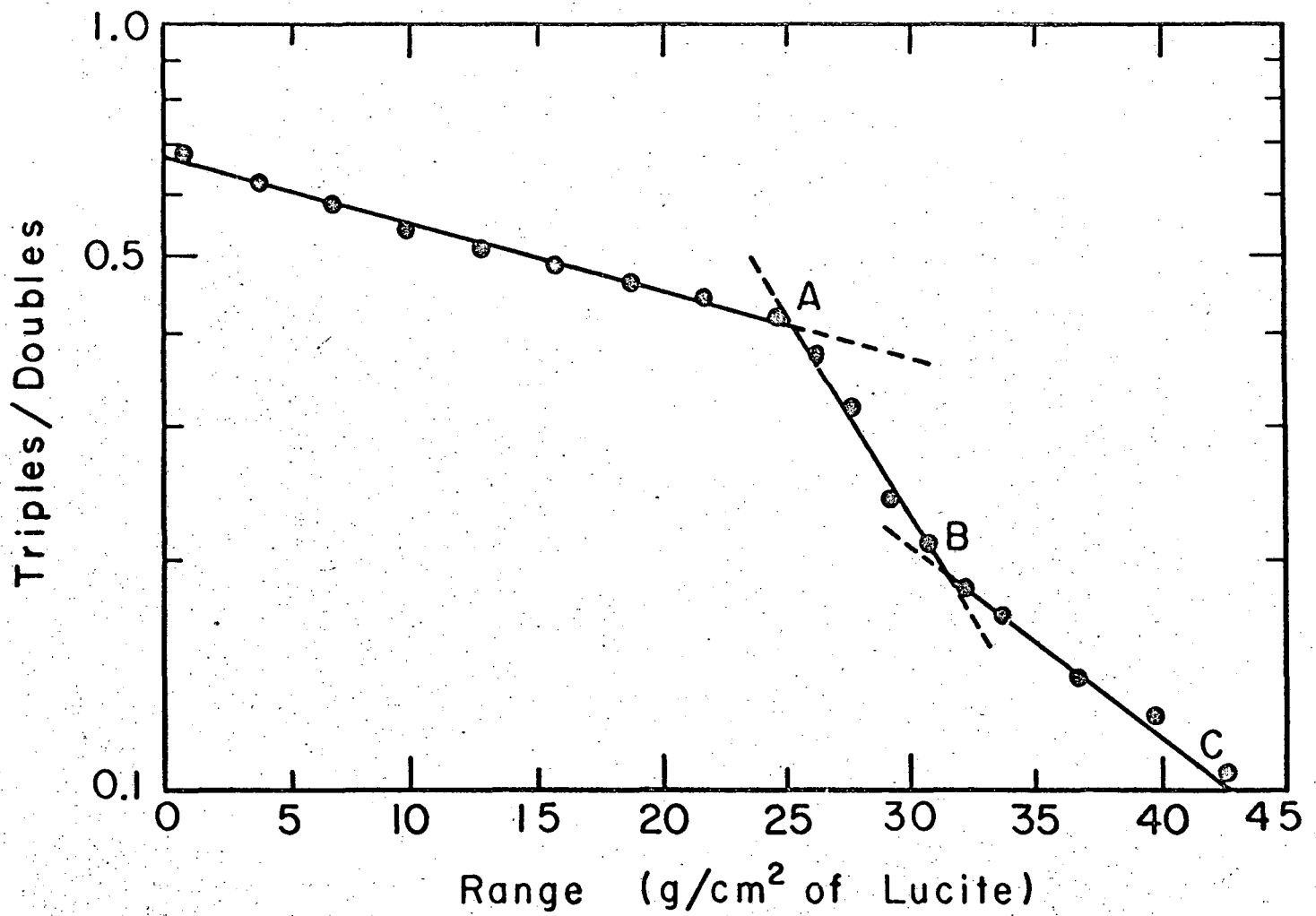
1.0
0.5
0.1
Triples / Doubles
0
5
10
15
20
25
30
35
40
45
Range (g/cm² of Lucite)
A
B
C

Fig. 5

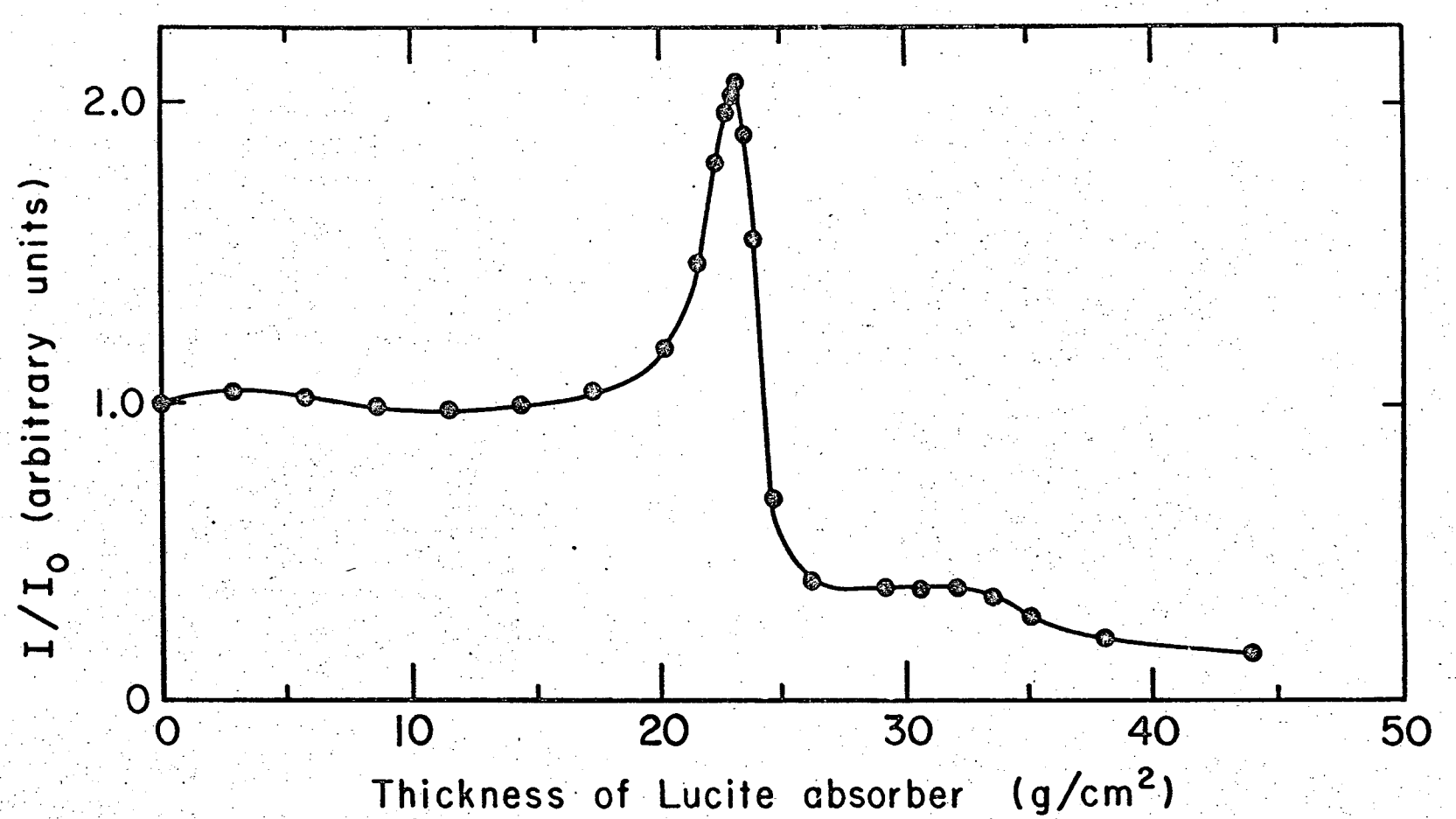
2.0
1.0
0
I/I$_0$ (arbitrary units)
0
10
20
30
40
50
Thickness of Lucite absorber (g/cm^2)

Fig. 6

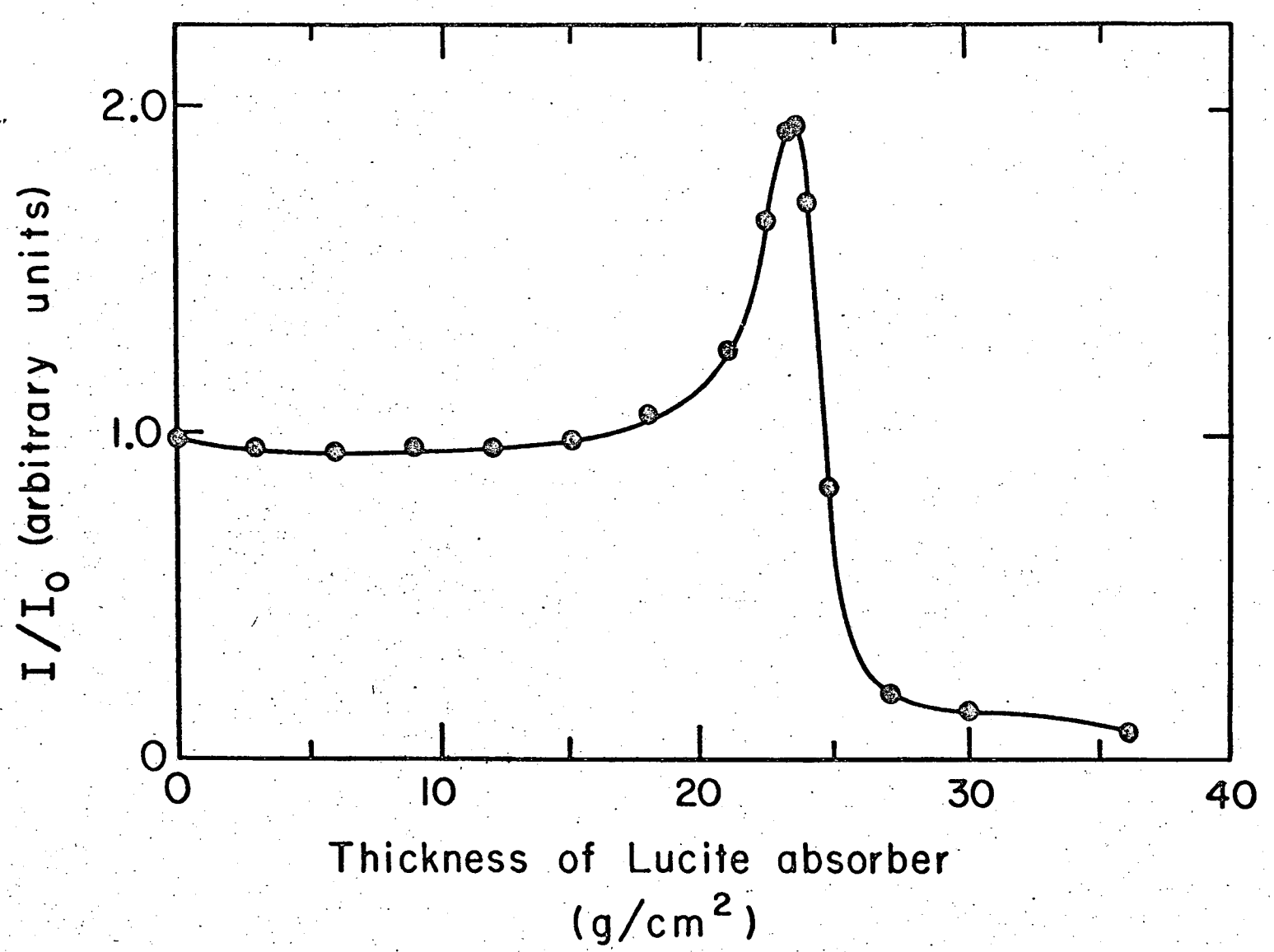
2.0
1.0
0
I/I$_o$ (arbitrary units)
0
10
20
30
40
Thickness of Lucite absorber
(g/cm^2)

Fig. 7

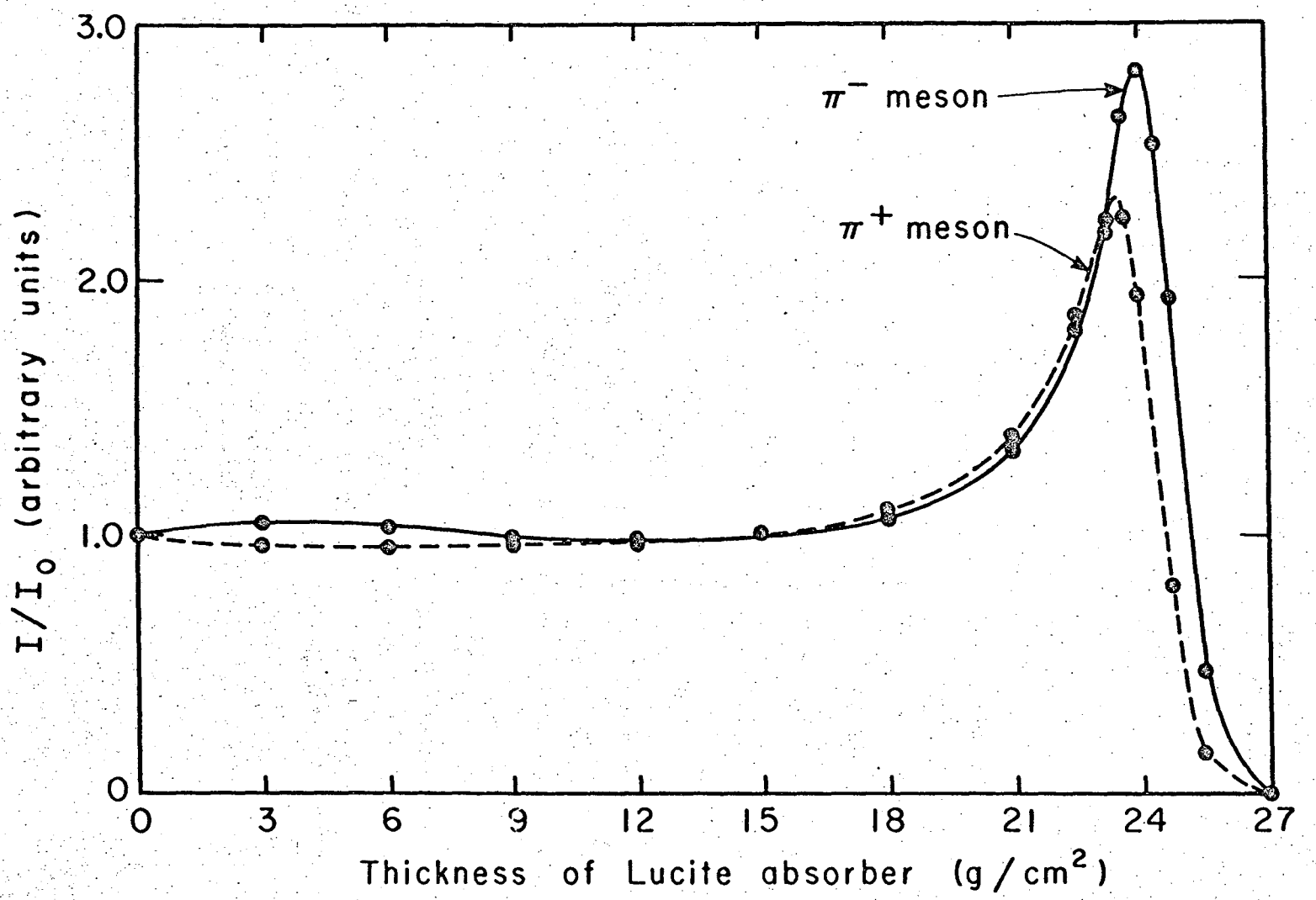
3.0
2.0
1.0
0
I/I_0 (arbitrary units)
π^- meson
π^+ meson
0
3
6
9
12
15
18
21
24
27
Thickness of Lucite absorber (g/cm^2)

Fig. 8

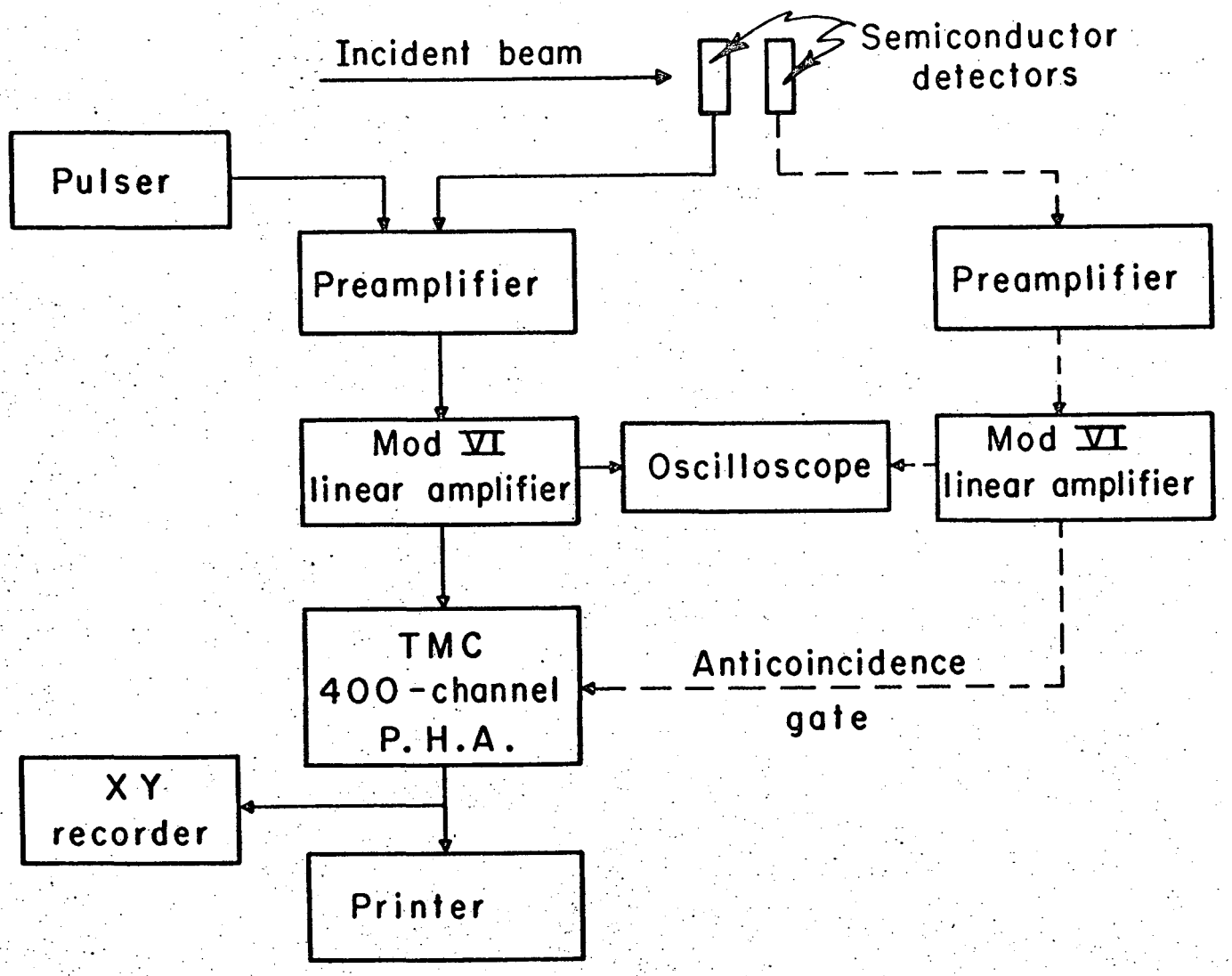
Incident beam
Semiconductor detectors
Pulser
Preamplifier
Preamplifier
Mod VI linear amplifier
Oscilloscope
Mod VI linear amplifier
TMC 400-channel P.H.A.
Anticoincidence gate
XY recorder
Printer

Fig. 9

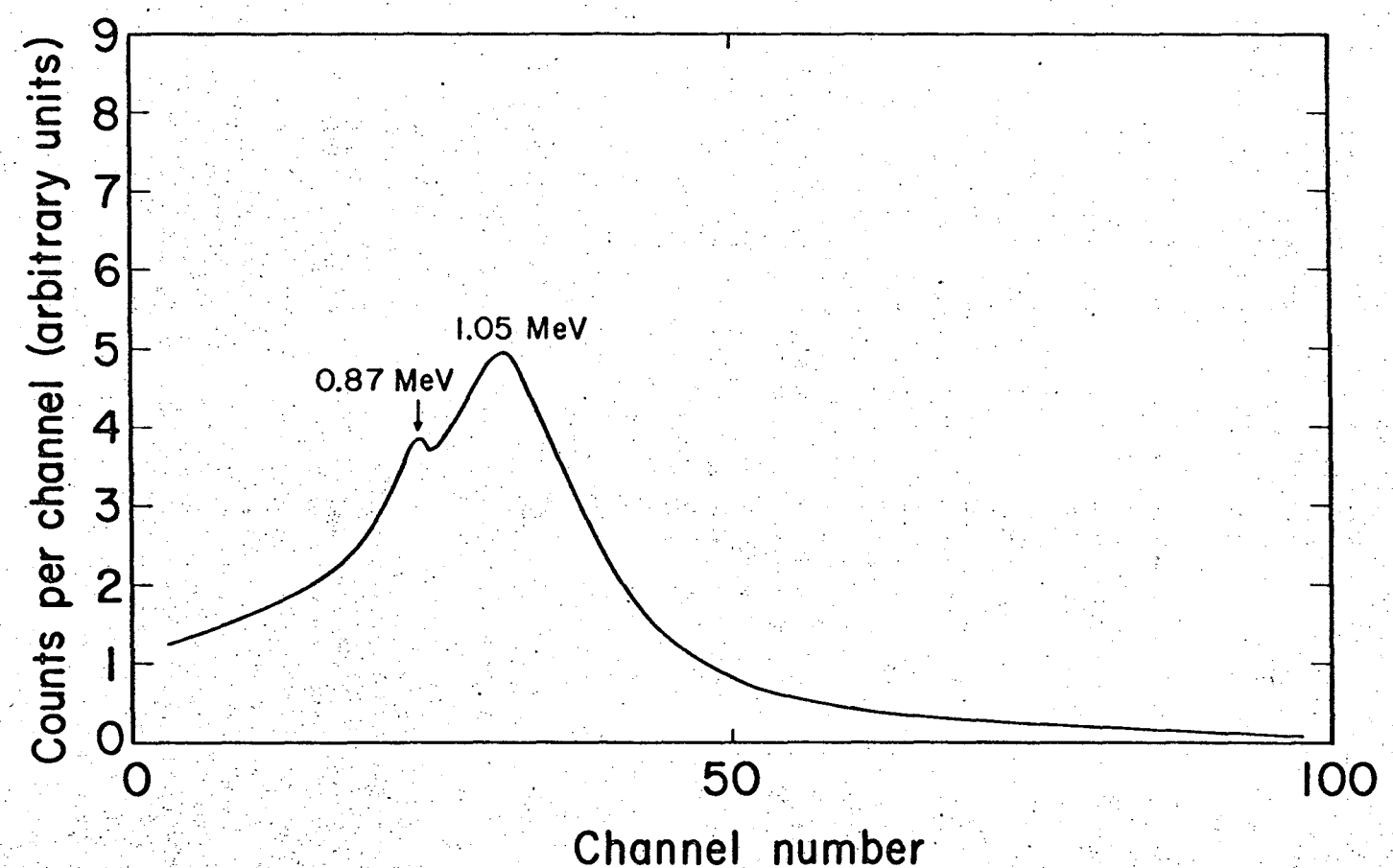
Counts per channel (arbitrary units)
0
1
2
3
4
5
6
7
8
9
0.87 MeV
1.05 MeV
0
50
100
Channel number

Fig. 10

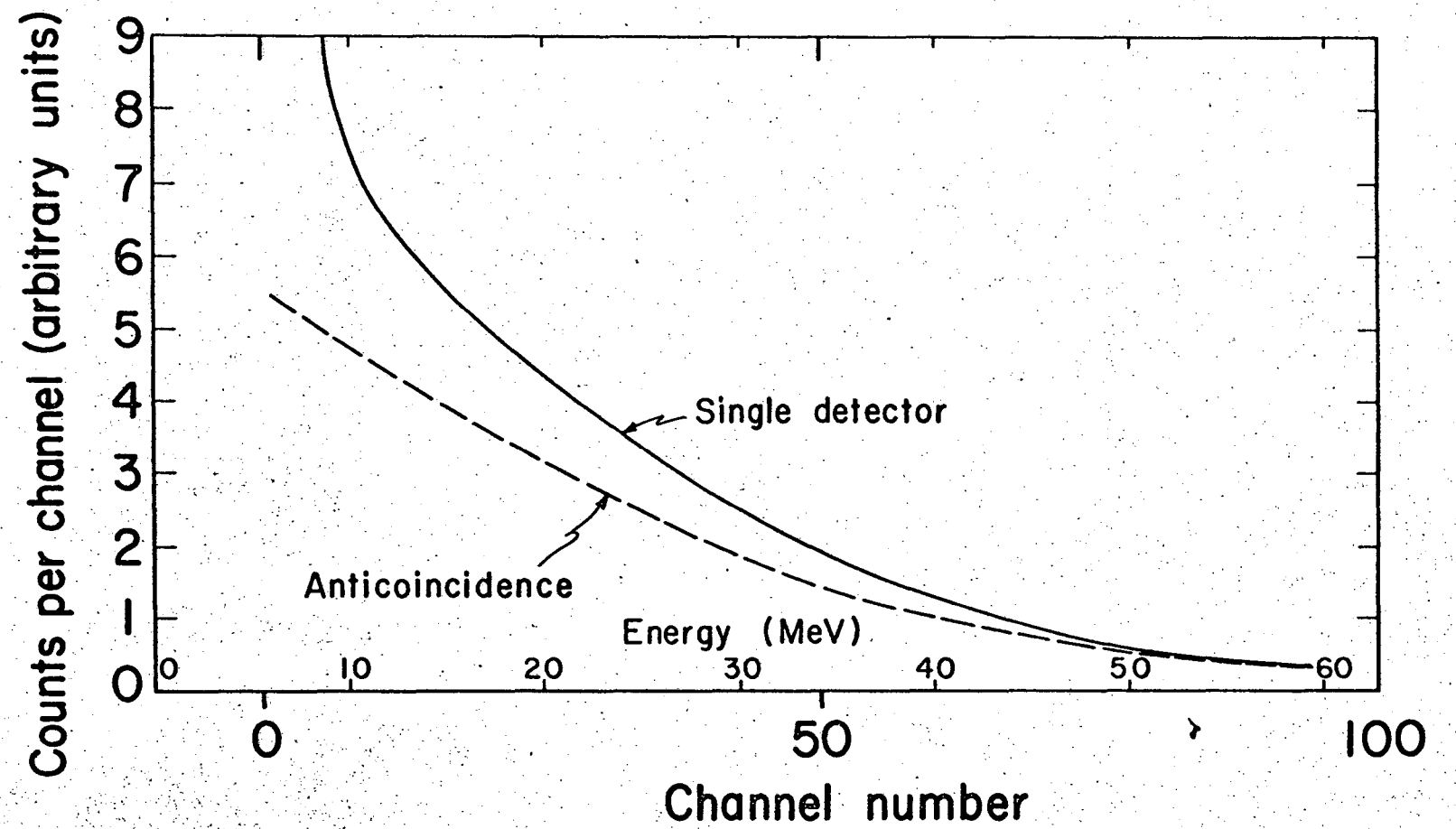
Counts per channel (arbitrary units)
9
8
7
6
5
4
3
2
1
0
Single detector
Anticoincidence
Energy (MeV)
0
10
20
30
40
50
60
0
50
100
Channel number

Fig. 11

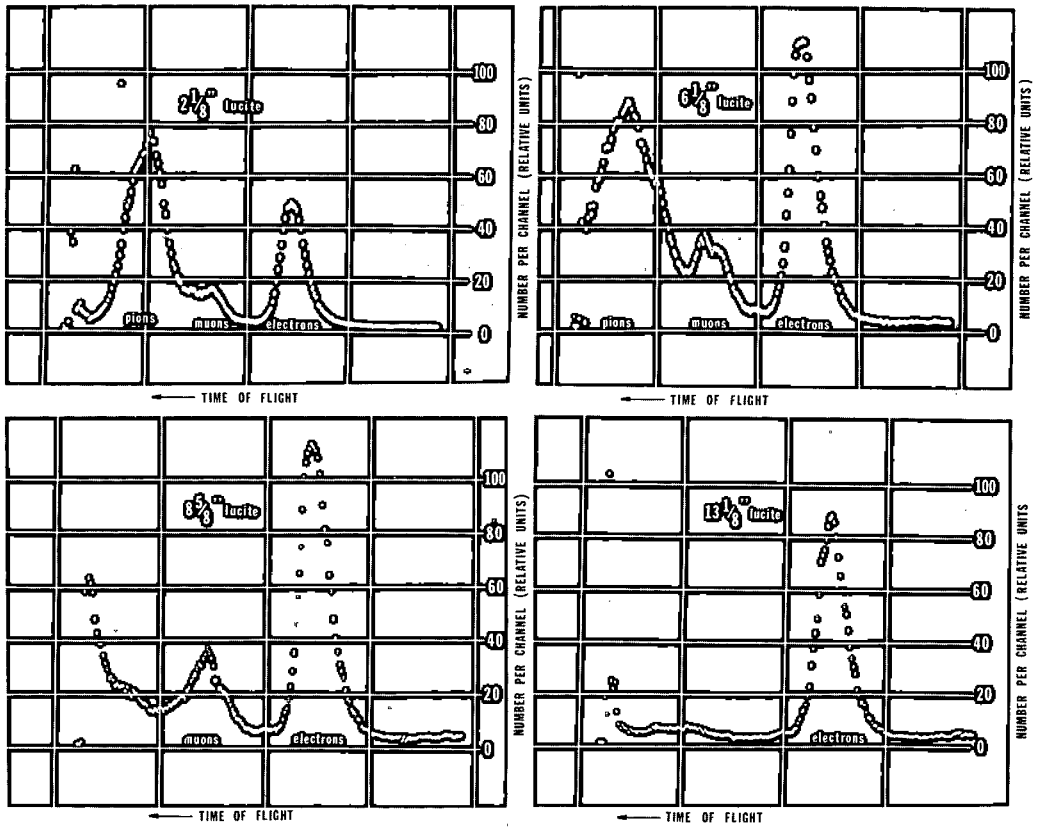

ZN-5090

Fig. 12

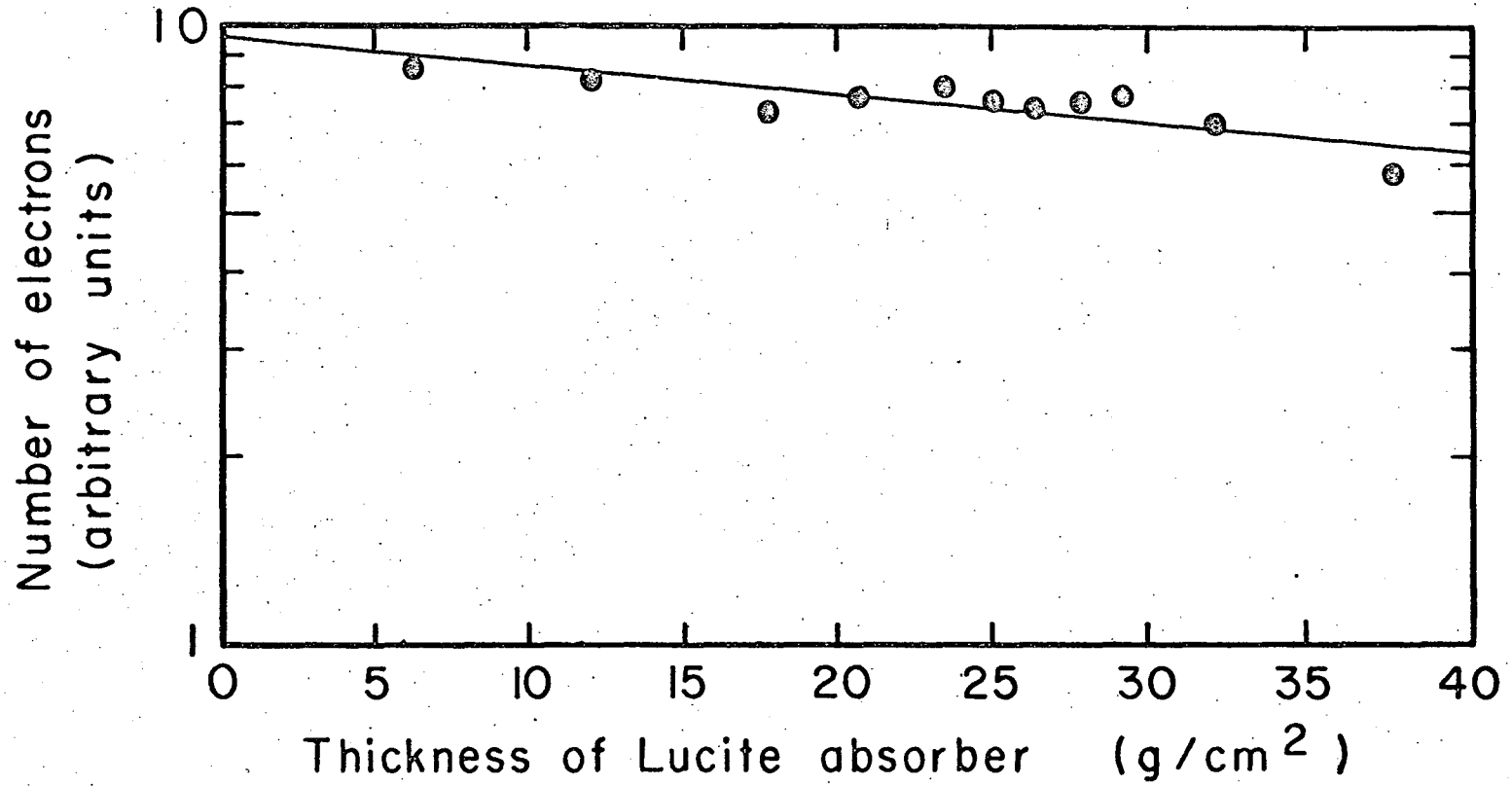
10
1
Number of electrons
(arbitrary units)
0
5
10
15
20
25
30
35
40
Thickness of Lucite absorber (g/cm 2)

Fig. 13

This report was prepared as an account of Government sponsored work. Neither the United States, nor the Commission, nor any person acting on behalf of the Commission:

A. Makes any warranty or representation, expressed or implied, with respect to the accuracy, completeness, or usefulness of the information contained in this report, or that the use of any information, apparatus, method, or process disclosed in this report may not infringe privately owned rights; or

B. Assumes any liabilities with respect to the use of, or for damages resulting from the use of any information, apparatus, method, or process disclosed in this report.

As used in the above, "person acting on behalf of the Commission" includes any employee or contractor of the Commission, or employee of such contractor, to the extent that such employee or contractor of the Commission, or employee of such contractor prepares, disseminates, or provides access to, any information pursuant to his employment or contract with the Commission, or his employment with such contractor.